ACSNANO

www.acsnano.org

ARTICLE

Accelerated Ultrafast Magnetization Dynamics at Graphene/CoGd Interfaces

Sucheta Mondal, Yuxuan Lin, Debanjan Polley, Cong Su, Alex Zettl, Sayeef Salahuddin, and Jeffrey Bokor*

Cite This: *ACS Nano* 2022, 16, 9620–9630

Read Online

ACCESS | Metrics & More | Article Recommendations | Supporting Information

ABSTRACT: **Atomically thin graphene layers can act as a spin-sink material when adjacent to a nanoscale magnetic surface. The enhancement in the extrinsic spin−orbit coupling (SOC) strength of graphene plays an important role in absorbing the spin angular momentum injected from the magnetic surface after perturbation with an external stimulus. As a result, the dynamics of the excited spin system is modified within the magnetic layer. In this paper, we demonstrate the modulation of ultrafast magnetization dynamics at graphene/ferrimagnet interfaces using the time-resolved magneto-optical Kerr effect (TRMOKE) technique. Magnetically modified interfaces with a systematic increase in the number of graphene layers coupled with the 10 nm-thick $Co_{74}Gd_{26}$ layer are studied. We find that the variation in the dynamical parameters, i.e., ultrafast demagnetization time, remagnetization times, decay time, effective damping, precessional frequency, etc., observed at different time scales is interconnected. The demagnetization time and decay time for the ferrimagnet become approximately two times faster than the corresponding intrinsic values. We found a possible correlation between the demagnetization time and damping. The effect is more pronounced for the interfaces with monolayer graphene and graphite. The spin-mixing conductance is found to be approximately 0.8 × 10^{15} cm^{-2}. The effect of SOC, pure spin current, the appearance of structural defects, and thermal properties at the graphene/ferrimagnet interface are responsible for the modifications of several dynamical parameters. This work demonstrates some important properties of the graphene/ferrimagnet interface which may unravel the possibilities of designing spintronic devices with elevated performance in the future.**

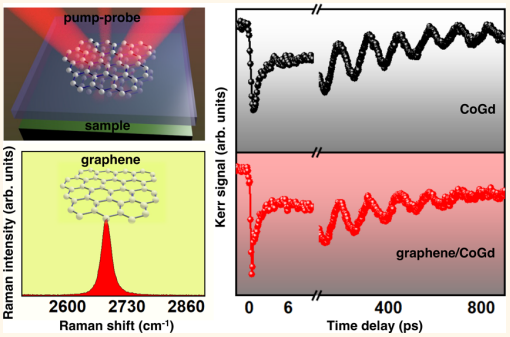

KEYWORDS: *graphene, ferrimagnet, TRMOKE, ultrafast demagnetization, precessional dynamics, spin current*

In the recent past, a significant surge was observed in research exploring the spin-dependent physical properties of graphene[1−3] and graphene-based magnetic heterostructures.[4,5] The field, "graphene-spintronics",[6] has emerged following the trail of the seminal works on isolation of graphene.[7,8] This wonder-material exhibits several exciting electronic properties,[9−11] such as zero bandgap, high electron mobility, low resistivity, excellent thermal conductivity, and gate tunable spin transport. Graphene is also very robust to environmental degradation. Nearly decoupled two-dimensional (2-D) graphene sheets can be stacked to form bilayer-, trilayer-, few layer-graphene (FLG), and then multilayer graphene (or graphite). The twisted-stack ordering is most common for the bilayer graphene. Beyond two layers, the ordering becomes arbitrarily complex. With an increasing number of layers, the linearly dispersive band structure of graphene starts showing band overlapping, splitting, and zone folding.[12] This modifies the physical properties of graphene. The intrinsic spin−orbit coupling (SOC) for monolayer graphene is weak, while for graphite the value becomes one order of magnitude higher.[13] Because of this weak SOC, long spin-diffusion length and spin-relaxation time in graphene[1,3] are observed. These properties are suitable for specific applications. Over the years, scientists have increasingly sought to harness the functionalities of graphene by increasing this SOC strength externally. Several theoretical and experimental methods are proposed such as adsorption,[14,15] proximity effects from an adjacent semimetal,[16] and hybridization with magnetic surfaces.[17−19] Increasing the SOC strength by engineering the graphene surface often leads to opening of

Received: March 23, 2022
Accepted: June 7, 2022
Published: June 13, 2022

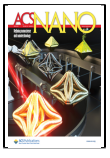

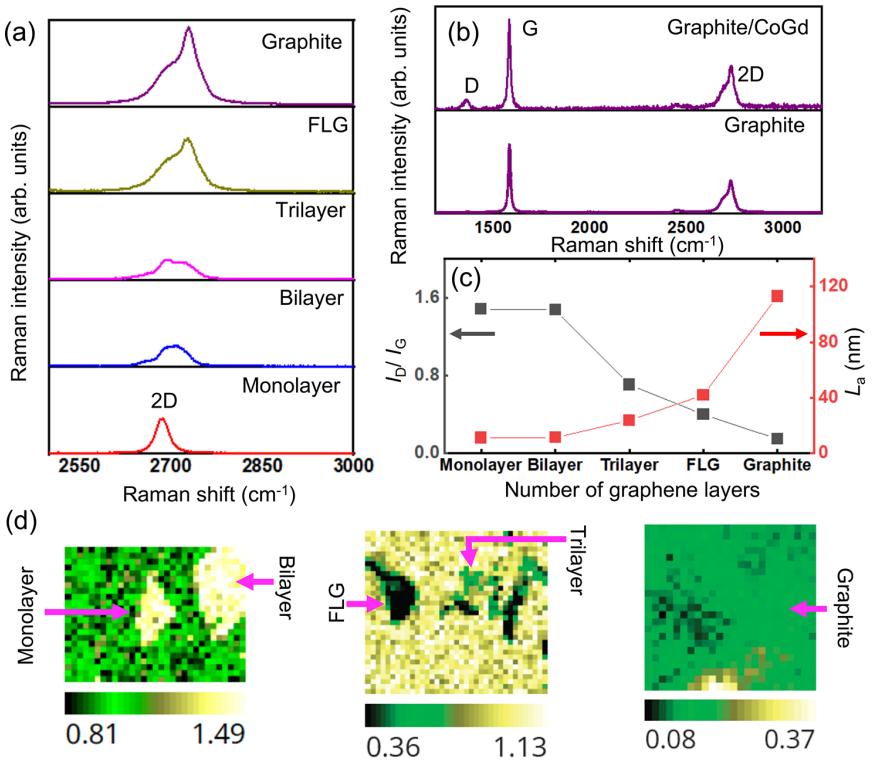

Figure 1. (a) Micro-Raman spectra showing 2D peaks for the graphene flakes transferred on Si/SiO_2 substrate. The number of layers is indicated inside the figure. (b) Micro-Raman spectra for the graphite flake obtained before and after deposition of CoGd (10 nm)/Ta (4 nm). Relevant peaks are identified and marked accordingly. (c) The variation in the ratio between Raman intensities for D and G peaks (I_D/I_G) and the average distance between neighboring defects (L_a) with different graphene layers. The error bars lie inside the data points. (d) Spatial distribution of I_D/I_G obtained from the Raman mapping. Corresponding color bars are indicated below the images. The uniform color contrast within each flake represents the uniform distribution of defect densities across the surface. The images are not to scale.

the band gap and introduction of localized states near the Fermi level. In particular, charge transfer due to the strong hybridization between the dz^2 state of a ferromagnetic atom and the $p_z\pi$ state of graphene is reported.[20] In this process, the net magnetic moment of the ferromagnet is reduced due to additional spin polarization in the graphene layers. With such advancements, this multifunctional 2-D material may even be envisioned as a latent substitute for three-dimensional heavy metals in magnetic multilayers. Graphene can generate pure spin current or spin-polarized current as evidenced from the quantum spin Hall effect,[21] Rashba effect,[14] and spin Seebeck effect[22] reported so far. The spin transport in graphene/ferromagnet heterostructures across the lateral[1] and vertical dimensions[23] is investigated by using local and nonlocal measurement techniques. Significantly, the spin-pumping effect, which does not necessarily require any charge current, is demonstrated for monolayer graphene and graphite.[19,24,25] An inverse relationship between damping and demagnetization time is established in the graphene/CoFeB interface from time-resolved magneto-optical Kerr effect (TRMOKE) microscopy measurements.[25] The modulation in the Gilbert damping shows dependence on the spin-mixing conductance and spin transparency of the interface in the presence of graphene similar to other conventional heavy metals.[26] The dynamics of Permalloy adjacent to graphene grown by the chemical vapor deposition method was also studied using ferromagnetic resonance techniques.[27] However, a comprehensive study of dynamical properties of a magnetic system with an increase in the number of graphene layers is lacking.

In the mechanical exfoliation process, which is so far the most successful and convenient method for layer-by-layer transfer of graphene onto a substrate, the flake size varies up to few tens of microns. This may introduce complexities in subsequent sample fabrication steps due to the uncertainty in shape, size, and position of the flakes embedded on a RF waveguide. Besides that, the graphene/metal interface suffers from impedance mismatch problems in electrical spin-pumping measurements. Most of these ambiguities are eliminated while probing ultrafast magnetization dynamics directly in the time domain by exploiting optical pump−probe techniques[28,29] with improved spatiotemporal resolution. The values of dynamical parameters including damping extracted via a noninvasive and localized optical method are marginally affected by contribution from spatial inhomogeneities unlike the global electrical measurements.

It is pertinent to mention that many studies are reported on the graphene/ferromagnet system from various aspects. However, research focusing on the graphene/ferrimagnet interface is yet to escalate. Ultrafast magnetization dynamics becomes more intriguing in the case of ferrimagnets due to exchange of angular momentum between the antiferromagnetically coupled nonequivalent sublattices. The ferrimagnetic alloys of rare earth (RE) and transition metal (TM) exhibit tunable magnetic properties with the change in composition.

https://doi.org/10.1021/acsnano.2c02899
ACS Nano 2022, 16, 9620−9630

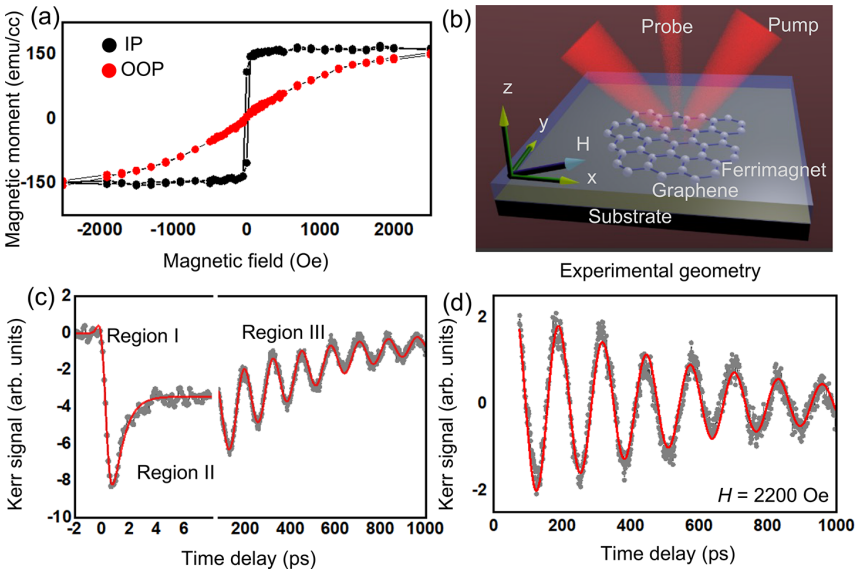

Figure 2. (a) The IP and OOP hysteresis loops for substrate/CoGd (10 nm)/Ta (4 nm) obtained from VSM. (b) Schematic of TRMOKE geometry. Dimensions of the layers and laser spots are not at scale. (c) Typical TRMOKE trace for substrate/CoGd (10 nm)/Ta (4 nm). The three temporal regions are specified within the graph. The data are measured at H = 2200 Oe. (d) The background-subtracted Kerr signal in Region-III.

The net magnetic moment is lower, and damping is reportedly higher in such systems compared with ferromagnets. Specifically, the Gd-based ferrimagnets are popular candidates for probing ultrafast demagnetization,[30] spin precession,[31,32] all-optical switching,[33,34] and picosecond electrical-pulse induced switching.[35] Recently, successful helicity independent, all-optical toggle switching is demonstrated in submicron-sized optomagnetic tunnel junctions with a perpendicularly magnetized Gd-based free layer.[36,37] All of these efforts demonstrate the usefulness of Gd-based ferrimagnets for the spintronic applications in the future.

In this work, we have investigated modulation of ultrafast magnetization dynamics by using the TRMOKE technique on graphene/ferrimagnet interfaces. A 10 nm-thick in-plane (IP) magnetized $Co_{74}Gd_{26}$ (CoGd here on) layer is deposited on top of mechanically exfoliated monolayer-, bilayer-, trilayer-, FL-graphene, and graphite flakes. The dynamical parameters extracted from time-resolved Kerr signals vary non-monotonically with the number of graphene layers. The demagnetization time (in femtosecond time scale) and decay time (in nanosecond time scale) of the ferrimagnet become approximately two times faster in the presence of the graphene layers. The variation in fast and slow demagnetization times indicates activation of different energy distribution channels with an increasing number of graphene layers. The remagnetization processes in the picosecond and sub-nanosecond time scales also become modified. It is noteworthy that all-optical excitation and detection of spin-pumping effects in CoGd-based multilayers have not been reported so far. Our experimental findings suggest that the spin-pumping effect at the graphene/CoGd interfaces is responsible for modulation of the effective damping. We believe that these modulations originate at the magnetically modified interfaces due to hybridization of the orbitals near the Fermi surface.[38] We particularly emphasize the role of pure spin current, the presence of defects in the graphene layers, and their thermal properties to be key factors to influence the ultrafast dynamics of CoGd on graphene.

RESULTS AND DISCUSSION

The graphene layers are mechanically exfoliated on top of a Si/SiO_2 substrate. A 10 nm-thick CoGd film is sputtered on top of the graphene layers using a DC magnetron sputtering. The film is capped with 4 nm-thick Ta to prevent the surface from environmental degradation. Raman spectroscopy measurements are performed to characterize the properties of graphene flakes before and after the deposition of CoGd. A single Lorentzian peak of the 2D band (Raman shift ∼2684 cm^{-1}) corresponds to monolayer graphene (Figure 1a). Then, the systematic evolution from bilayer graphene to graphite is identified from the definite shape asymmetry of the 2D peaks,[39] which is due to the overlay of double resonance peaks from the increased number of sub-bands as the layer number increases. Microscope images reveal that the optical contrasts are different for different graphene layers (see Supporting Information). The sizes of the flakes vary roughly from ∼5 to ∼15 μm. The variation in relative Raman intensities between the 2D and bulk G (∼1587 cm^{-1}) peaks (I_{2D}/I_G) helps further to identify the number of graphene layers (see Supporting Information).[40] Immediately after exfoliation, there is no defect peak (D) observed, which indicates the high quality of the graphene layers. Deposition of CoGd results in the appearance of growth-induced defects. The comparison between the two Raman spectra for the graphite flake is explicitly shown in Figure 1b where the D peak resides at ∼1339 cm^{-1} energy. The ratio between D peak intensity (I_D) and I_G is decreased from ∼1.5 to ∼0.1 with the number of graphene layers (Figure 1c). Therefore, the calculated average distance between the neighboring defects (L_a) is found to be increased 10 times for graphite in comparison to monolayer graphene (see Supporting Information). This signifies that due to bombardment with heavy atoms on the interface during

https://doi.org/10.1021/acsnano.2c02899
ACS Nano 2022, 16, 9620−9630

sputtering defects appear in the graphene layers, and the defect concentration reduces gradually with increasing numbers of graphene layers. We have also performed spatial mapping of the defect density by keeping all other experimental conditions same as the single-point Raman measurement. The I_D/I_G, which is proportional to the defect density, decreases with increasing numbers of graphene layers. In Figure 1d, the uniform color contrast within each flake represents uniform distribution of defects across the surface of the flakes which only scales with graphene layer thickness. The surface properties are investigated by using the atomic force microscopy (AFM) technique in noncontact mode. The average roughness is found to be ∼0.8 nm for the film. Detailed discussion on the roughness and thickness of the sample in the presence of graphene layers can be found in the Supporting Information.

The IP and out-of-plane (OOP) hysteresis curves obtained from vibrating sample magnetometry (VSM) show that the saturation magnetization (M_s) for bare 10 nm-thick CoGd film is ∼150 emu/cm^3 (Figure 2a). The IP and OOP saturation fields are ∼50 Oe and ∼2000 Oe, respectively. The small coercivity and nature of magnetic reversal observed for this film refer to the absence of any significant anisotropy. Time-resolved magnetization dynamics is measured in a substrate/CoGd (10 nm)/Ta (4 nm) film by using the single-color pump−probe-based TRMOKE technique. The experimental geometry is depicted in Figure 2b. The femtosecond pump pulse (fluence = 3.0 mJ/cm^2) is incident obliquely on the sample, whereas the probe beam (fluence = 0.5 mJ/cm^2) is focused inside the pump spot to collect the polar MOKE signal. A sufficiently large IP magnetic field (H > saturation field) is applied with a slight tilt (∼15°) in the OOP direction to ensure a finite demagnetizing field, which is modulated by the pump pulse to launch precession in the sample. Upon laser excitation, the electron temperature increases instantaneously, creating hot electrons above the Fermi level, which in turn excite the spin subsystem by electron−magnon interaction. The quenching of magnetization is known as ultrafast demagnetization,[28] which occurs within the first few hundreds of femtoseconds (demagnetization time: τ_m). Subsequently, the energy rebalancing between the electron-, spin-, and lattice-subsystems causes this quenched magnetization to relax back to its original equilibrium state. The time scale of electron−phonon interaction is known as the fast remagnetization time (τ_e), which is on the order of picoseconds. The effective anisotropy of the magnetic material also gets modified upon the excitation by the pump pulse. This exerts a torque on the magnetization and induces precession on top of slow remagnetization on a nanosecond time scale.[29] Within the slow remagnetization time (τ_l), the energy is dissipated from the lattice bath of the magnetic layer to the nonmagnetic layers and substrate. Figure 2c represents the time-resolved Kerr rotation data obtained for a substrate/CoGd/Ta (without graphene) sample showing three different temporal regions: ultrafast demagnetization (Region-I), fast remagnetization (Region-II), and slow remagnetization superposed with damped precession (Region-III). The ultrafast demagnetization data are fitted with the phenomenological three-temperature model,[41,42] which is widely used (see Supporting Information). The τ_m and τ_e for CoGd are found to be ∼300 fs and ∼800 fs, respectively. The precessional dynamics is governed by the Landau−Lifshitz−Gilbert (LLG) equation.[43,44] The time-dependent magnetization data (M(t)) in Region-III is fitted with the following expression of a damped sinusoidal function with exponential background:

$$M(t) = M(0)(Ae^{-t/\tau_l} + Be^{-t/\tau_d}\sin(2\pi ft + \phi)) \quad (1)$$

A and B are multiplication factors to match the signal amplitude. Figure 2d shows the background-subtracted precessional data. From the fit, the decay time (τ_d) and precessional frequency (f) are found to be ∼0.5 ns and ∼8.0 GHz respectively for H = 2200 Oe. The frequency spectra are obtained after performing a fast Fourier transform (FFT) on the background-subtracted precessional data (Figure 3a). The

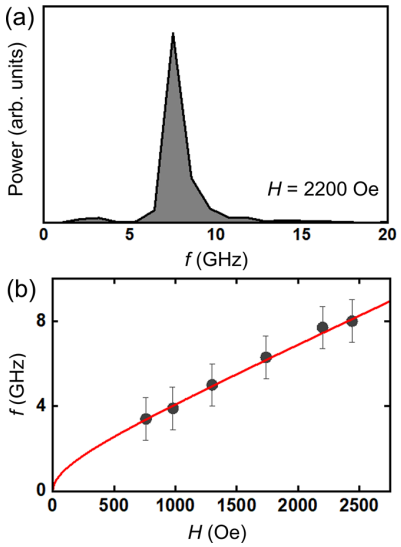

Figure 3. (a) The frequency spectra obtained from the background-subtracted Kerr signal for substrate/CoGd (10 nm)/Ta (4 nm) sample. The data are measured at H = 2200 Oe. (b) Bias magnetic field dependence of precessional frequency. The solid line corresponds to the Kittel fit.

line width of the peak (at ∼7.8 GHz) results from the limited experimental time window (∼1 ns) and high damping of the precessional data. The frequency values obtained in the time domain and frequency domain corroborate with each other. In practice, the stability of the spin-wave modes and appearance of any nonmagnetic mode can be validated by studying the field dependence of the frequency spectra. In this sample, a single precessional mode is identified with the highest intensity and stability. The effective magnetization (M_{eff}) within the probed area of the sample is calculated from the field dependence of this fundamental mode frequency. The data points in Figure 3b are fitted with the widely used Kittel formula:[45]

$$f = \frac{\gamma}{2\pi}\sqrt{H(H + 4\pi M_{eff})} \quad (2)$$

Here, γ is the gyromagnetic ratio. M_{eff} obtained from this fit (∼120 emu/cm^3) agrees well with the value of M_s obtained from the VSM measurement. Also, no evidence of any significant anisotropy is found in this 10 nm-thick amorphous CoGd film in contrast to thinner ferromagnetic films.[25] The effective damping (α_{eff}) of this film is calculated by using the following formula:[45]

https://doi.org/10.1021/acsnano.2c02899
ACS Nano 2022, 16, 9620−9630

$$\alpha_{\text{eff}} = \frac{1}{\tau_d \gamma (H + 2\pi M_{\text{eff}})} \quad (3)$$

α_{eff} contains all the contributions from intrinsic and extrinsic damping in the system. The values α_{eff} ($\geq$0.03) for the CoGd film within our experimental field regime are close to the reported value ($\sim$0.10) in the literature.[46]

In the presence of graphene underlayers, the dynamical properties of CoGd are strongly modified due to hybridization at the interface. Figure 4a shows ultrafast demagnetization data

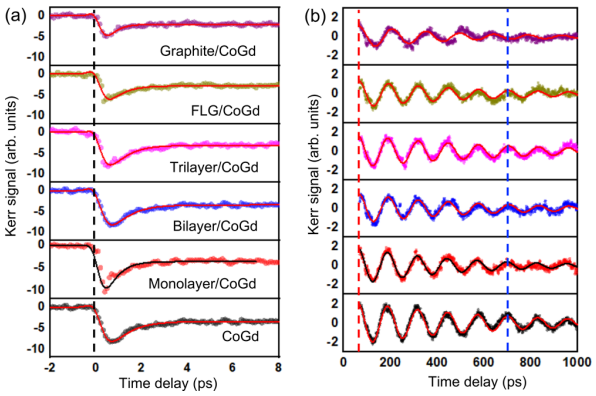

Figure 4. (a) Ultrafast demagnetization, fast remagnetization, and (b) magnetization precession measured using the TRMOKE technique in substrate/graphene/CoGd (10 nm)/Ta (4 nm) sample on the flakes with the different numbers of graphene layers. The data are measured at H = 2200 Oe. The solid lines correspond to the fits. The dotted line in the left-hand side panel represents the zero-delay position between pump and probe pulses. The decrease in the frequency of graphite/CoGd is identified from the reduction in the number of oscillations within the time window of about 700 ps marked by the two dotted lines directly in the time domain.

for substrate/graphene (mono-, bi-, tri-, few-layers, and graphite)/CoGd/Ta samples. The demagnetization data are initially recorded for both polarities of H. Later, those results are subtracted and processed in the conventional manner. Finally, the experimental data points are fitted with the three-temperature model. For all cases (from monolayer up to graphite), ultrafast demagnetization gets accelerated in comparison to the bare CoGd film. The fast remagnetization process also becomes faster. The amount of quenching of the magnetization reduces for CoGd with thicker graphene layers. Figure 4b clearly shows that the background-subtracted precessional signals decay at a faster rate for graphite/CoGd and monolayer graphene/CoGd in comparison to the others. Also, the precessional frequency seems to be lower for graphite/CoGd. Additionally, modification in the slow remagnetization process for CoGd with different graphene layers is evidenced from the difference in slopes of the exponential background in sub-nanosecond time scale (see Supporting Information).

Each FFT spectrum for graphene/CoGd samples with different layer numbers accommodates one highly intense magnetic mode and few low-intensity modes having a nonmagnetic origin. Figure 5a shows more clearly that the peak frequencies appear close to ~7.8 GHz for all of the flakes. However, the peak becomes more asymmetric and inclines toward the low-frequency side for CoGd with thicker graphene

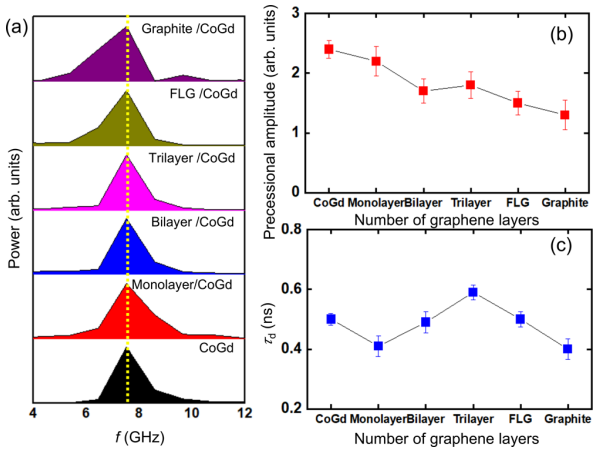

Figure 5. (a) The frequency spectra obtained for the substrate/graphene/CoGd (10 nm)/Ta (4 nm) sample with different number of graphene layers. The dotted line corresponds to the peak frequency of the fundamental mode in the bare CoGd film. (b) The variation in precessional amplitude and (c) decay time of CoGd with different numbers of graphene layers obtained by fitting the oscillatory time-resolved Kerr signal. All of the measurements were done at H = 2200 Oe. The lines are a guide to the eye.

layers. This slight red shift (~0.8 GHz) observed both in the time domain and frequency domain indicates possible reduction in the interfacial magnetic moment. The amplitude of precession also decreases gradually (Figure 5b). Because of symmetry matching and orbital overlap, the d-band of the TMs can get modified with pd hybridization in the presence of graphene.[47] A strong spin-polarization effect and charge-transfer effect in graphene adjacent to the Co atoms are reportedly responsible for the reduction in magnetic moment of Co.[19] The values of line widths in FFT spectra are higher for CoGd in the presence of monolayer graphene and graphite. The τ_d obtained from the time domain data (which is inversely proportional to the line width in frequency domain) is more than 1.5 times smaller for both the flakes than that of bare CoGd film. The non-monotonic trend observed in Figure 5c indicates that the mechanisms responsible for the deviation of τ_d of CoGd from its intrinsic value do not scale with the number of graphene layers. The effects are more pronounced in the presence of graphene and graphite.

In Figure 6, the variation in the dynamical parameters for graphene/CoGd is plotted with the number of graphene layers. The intrinsic spin−orbit interaction for graphite is one order of magnitude larger than the monolayer due to the mixing between the π and σ bands by interlayer hopping.[13] This can be a possible reason behind the fact that dynamical parameters which are dependent on spin−orbit interaction sometimes exhibit an even larger change in the presence of graphite compared to monolayer graphene. However, in monolayer graphene on the magnetic surface, the extrinsic SOC strength is elevated.[18] Additionally, if the monolayer loses flatness, the extrinsic SOC can be further enhanced for the curved surface.[48] This can have a relatively stronger influence in comparison to bilayer-, trilayer-, and FL-graphene. The concentration of defects plays an important role to control the carrier transport at the interface on the picosecond time scale. In essence, the carrier- and spin-transport properties,

https://doi.org/10.1021/acsnano.2c02899
ACS Nano 2022, 16, 9620−9630

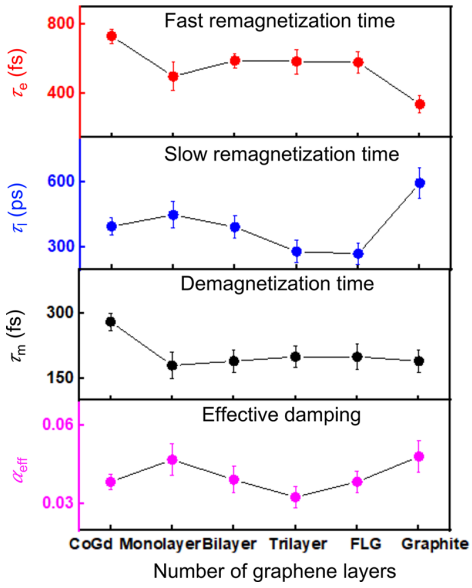

Figure 6. Variation of fast remagnetization time, slow remagnetization time, ultrafast demagnetization time, and effective damping with the numbers of graphene layers adjacent to the CoGd layer in the sample. The values are obtained from the fits of the time-resolved Kerr signal presented in Figure 4. The measurement was done at H = 2200 Oe. The lines are a guide to the eye.

which influence the dynamics of the graphene/CoGd system, depend largely on the quality of individual graphene layers as well as proximity-induced modifications at the interfaces.

The value of $\tau_e \approx 800$ fs for bare CoGd is determined by the electronic specific heat and coupling constants of the electron and lattice baths for Co and Gd. The $\tau_e \approx 400$ fs for CoGd in the presence of the graphene layers indicates that the energy from the electron bath can be dissipated via multiple cooling pathways. Several scattering processes involving optical phonon, acoustic phonon, plasmons, etc. are reported in graphene, which governs the carrier dynamics on a picosecond time scale.[49] Also, the relaxation of energy from monolayer graphene to the polar substrate, i.e., SiO_2, accelerates due to surface polar phonon modes. As defects play an important role in these 2-D materials, a disorder-assisted cooling mechanism is also proposed. This is supposed to be faster because of the low charge mobility due to enhancement in scattering events. Atomic defects are also known to modify the Fermi energy and band structure.[14,15] We infer that in addition to the interaction between electron and lattice bath, disorder or defect assisted cooling plays a key role in accelerating the dynamics at the graphene/CoGd interface. Additionally, the interfacial roughness is experimentally observed to be small in the presence of thicker graphite.[24] Therefore, the interface interaction may get stronger, and hence a larger modification can be evidenced due to creation of an additional dissipation channel during the fast remagnetization process.

The slow remagnetization process for CoGd is controlled by the energy dissipation from the CoGd lattice to the adjacent graphene layers and then to the substrate on the sub-nanosecond time scale. Not only the thermal time constants (τ) of the individual graphene layers but also thermal impedance of each interface play very important roles. Experimental and theoretical studies have shown that thermal transport in graphene is phonon mediated.[50] The lattice specific heat (C_p) and thermal conductivity (κ) dominate the electronic contribution at all temperatures on longer time scales. These parameters largely vary when graphene is supported or encased with other layers. It is noteworthy that both the IP and cross-plane κ can be contributing factors for graphene-based multilayers. The IP κ of freely suspended graphene at room temperature is approximately 2000−4000 W m^{-1} K^{-1}, which is among the highest of any known material.[50] This fact promotes graphene as a high-quality "heat-sink" material. However, any additional disorder arising from the substrate/graphene interface or even residue from the sample fabrication process will introduce more phonon scattering.[51] This reduction is a common observation. The IP κ for Si/SiO_2/graphene decreases with the number of graphene layers. From bulk graphite ($\kappa \approx 1000$ W m^{-1} K^{-1}), it approaches the value for monolayer graphene ($\kappa \approx 100$ W m^{-1} K^{-1}) in a nonlinear fashion.[51] Despite relatively high IP κ, the heat flow in the vertical direction is strongly hindered in the graphene layers due to weak interplane van der Waals interaction.[52,53] This cross-plane κ is mostly constant up to a few layers of graphene.[52] The reported value of κ for pyrolytic graphite along the c-axis is 6 W m^{-1} K^{-1}, which approaches the thermal properties of SiO_2.[50] Such modification in thermal properties affects the response time of graphene-based multilayers. Along with this trade-off between the IP and the cross-plane thermal transport, the finite probability of phonon transmission should also be considered for each interface for a multilayer. The effective impedance to heat flow can be characterized by a property of an individual interface known as Kapitza thermal conductance (see Supporting Information).[54] In our experiment, the heat profile of the laser is Gaussian, and the penetration depth of the laser is comparable to the thickness ($\gtrsim$16 nm) of the graphene/CoGd/capping stack with monolayer graphene to FLG. We expect only a radial temperature gradient to influence the heat dissipation process for all the flakes except the thick graphite.[55] When the heat distribution in the cross-plane direction is uniform, it is possible that only IP κ at the SiO_2/graphene interface dominates the slow remagnetization process. As κ increases from monolayer graphene to FLG, the thermal transport is accelerated, and hence the τ_1 of CoGd gradually decreases (from 400 to 300 ps approximately). Being conductive and relatively thick, graphite can shield the laser before reaching the bottom interface with SiO_2. This creates a nonuniform heat gradient across the thickness of the stack and thermal conductance at multiple interfaces controls the energy transport. Because of a poor cross-plane κ and larger volume of the flake, the graphite/CoGd interface retains the heat for longer time, resulting in an almost two-time enhancement of τ_1 (~600 ps).

The value of $\tau_m \approx 300$ fs for the bare CoGd film primarily indicates a dominant contribution from the d-orbital of Co over the 4f orbital of the Gd which, would have resulted in slower dynamics. In the presence of graphene layers, ultrafast demagnetization ($\tau_m \approx 150$ fs) becomes about two times faster. Earlier studies in d-band TMs revealed that graphene strongly influences the energy of different orbitals of magnetic atoms evidenced from the calculated density of states.[38,56] For Co, the $3d_z^2$ and $3d_{x^2-y^2}$ states get swapped with each other. Because of symmetry reasons, the $3d_z^2$ states get shifted toward the Fermi level due to hybridization with $2p_z$ states of

https://doi.org/10.1021/acsnano.2c02899
ACS Nano 2022, 16, 9620−9630

graphene. The appearance of more allowed states and the change in exchange splitting for spin-up and spin-down electrons near Fermi level[56] may be the primary reason behind the reduction in the demagnetization time. The modification in density of states of a multi-sublattice system in the presence of graphene layers is expected to be more complex. On the other hand, graphene layers help to dissipate spin angular momentum from the magnetic layer via spin-flip scattering at the interface, resulting in accelerated dynamics.[2] Thus, spin transport between the magnetic and nonmagnetic layers may influence the demagnetization process. It is worth mentioning here that the growth of the magnetic layer on the flakes with different layer thickness can have a slight variation, which in turn can influence the demagnetization time. However, for this sample, all the graphene flakes are exfoliated on a single Si/SiO_2 substrate, and CoGd film is sputtered on top of those flakes at the exact same growth condition. We believe that the structural modifications which are more likely to introduce a monotonic change in the dynamics with an increasing number of graphene layers are not playing a dominant role in this experiment.

The injection of pure spin current from CoGd to graphene layers via spin pumping is the dominant contributor to the damping modulation. If a magnetic surface is in contact with a nonmagnetic material having reasonably strong SOC strength, then damping increases substantially due to strong scattering or absorbance of the pumped spins. In contrast, if the nonmagnetic material does not act as a spin sink, then pumped spins will accumulate at the interface before entering the nonmagnetic layer. This can drive a diffusive spin current back toward the magnetic layer in steady state. At this "spin battery limit", the spin-pumping effect gets nullified.[57] We have observed about 25% modulation in effective damping of CoGd in the presence of graphene layers. We believe that the interfaces with monolayer graphene and graphite in our experiments support the transport and absorption of angular momentum and hence increase the effective damping of the ferrimagnet. From the inverse relationship between the change in τ_m and α_{eff},[58] we have estimated the spin chemical potential (μ_s) for CoGd with monolayer graphene and graphite to be ~0.2 eV (see Supporting Information).[25,49,59] This is proportional to the spin accumulations at the graphene/CoGd interface, which may contribute to the ultrafast demagnetization process according to the diffusive spin-transport model. In contrast, dominance of the spin-flip scattering mechanism within the magnetic layer usually leads to a proportional relationship between the τ_m and α_{eff}.[60] It is pertinent to mention that the spin transport along the *c*-axis of graphene is different than the IP direction. The electrical conductivity, band matching, strength of spin−orbit interaction, presence of defects, and interfacial roughness collectively determine the spin-mixing conductance (G_{eff}) and hence the spin transparency at the interface. We have estimated $G_{eff} \approx 0.8 \times 10^{15}$ cm^{-2} for CoGd with graphene and graphite layers (see Supporting Information). The value suggests that those interfaces are moderately transparent to the spin current.[25,26] On the other hand, CoGd interfaces with bilayer-, trilayer-, and FL-graphene seem to be less transparent allowing a relatively smaller (or no) increase in the damping values. From first principle calculations and tight binding investigations, researchers have argued that the SOC in bilayer graphene mainly originates from the intralayer interaction and is weak in contrast to some of the earlier studies that predicted large interlayer effects.[13,61] In a FLG/TM junction with compromised electrical properties, spin-flip scattering is found to be responsible for reduced spin-injection efficiency.[62] Additionally, the possibility of spin-current blocking by a raised potential barrier at the SiO_2/graphene interface for some of the flakes cannot be ruled out. Interestingly, a strongly suppressed spin transport is also reported for monolayer graphene along the *c*-axis.[23,57] This is contrary to our experimental findings. We believe the growth conditions and measurement procedures followed in those studies are very diverse and cannot be directly compared with our observations. Additionally, spin transparency of the interface can be precisely determined by varying the thickness of the magnetic layer systematically for a constant thickness of the 2-D material. Such experimental demonstration is beyond the scope of this paper.

From the bias magnetic field dependence of damping (Figure 7a), we notice that damping values increases in the low field regime. This indicates a stronger presence of extrinsic factors originated from impurities, defects, magnetic inhomogeneity within the bulk of CoGd layer and at the interfaces,[25,26,32] etc. Sometimes, field-dependent modifications point toward the presence of magnon−magnon scattering in the system.[63] However, that effect increases with field, which is contrary to our observations. Also, this effect is small for graphene/magnet bilayers with thicker magnetic layers. Detailed discussion can be found in the Supporting Information. These contributions are difficult to quantify for such 2-D materials by varying the number of layers, as the physical properties of the layers are very diverse for both lateral and vertical dimensions. In our experiment, the application of a sufficiently large magnetic field is expected to eliminate most of these field-dependent extrinsic effects. This allows a fair comparison for the damping by varying the number of graphene layers at the higher field regime (Figure 7b). This

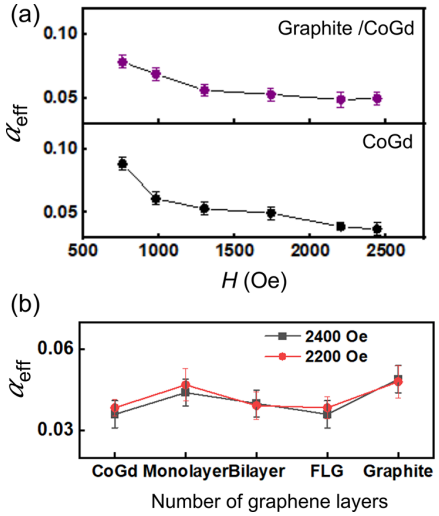

Figure 7. (a) Bias magnetic field dependence of the effective damping for bare CoGd and graphite/CoGd samples. (b) Variation of effective damping of CoGd with the number of graphene layers for H = 2200 and 2400 Oe. The lines are a guide to the eye.

https://doi.org/10.1021/acsnano.2c02899
ACS Nano 2022, 16, 9620−9630

comparison strongly supports our claims on modulated spin dynamics of CoGd in the presence of graphene layers.

CONCLUSION

We have investigated the modulation in ultrafast demagnetization, remagnetization, and damping in the presence of graphene layers underneath a ferrimagnet. Time-domain detection of the polar MOKE signal facilitates error-free determination of the dynamical parameters with different magnetic field strengths. We have created magnetically modified interfaces between the graphene and ferrimagnet, which is evidenced by the reduction in effective moment and precessional frequency. A non-monotonic variation in the dynamical parameters is observed for CoGd hybridized with monolayer-, bilayer-, trilayer-, FL-graphene, and graphite. In addition to the interaction between electron and lattice baths, disorder or defect-assisted cooling is found to reduce the fast remagnetization time up to two times at the graphene/CoGd interface. A phonon-mediated thermal transport mechanism is found to dominate the energy dissipation process at sub-nanosecond time scale. Because of modification in the thermal impedance of the individual layers and interfaces arising from the IP and cross-plane heat transport, the slow remagnetization time exhibits about 50% modulation. The extrinsic SOC of graphene layers arising from the proximity effect while being adjacent to the ferrimagnet plays a very crucial role. The ultrafast demagnetization of CoGd is found to be accelerated in the presence of graphene layers. One possible reason behind a noticeable reduction in demagnetization time can be the appearance of more allowed energy states near the Fermi level due to pd hybridization at the graphene/CoGd interface. An inverse dependence of demagnetization time with damping points toward the opening of additional energy dissipation channels for the angular momentum transport due to spin-pumping effect. We have observed about 25% modulation in the effective damping at graphene/CoGd interfaces in the high field regime. We believe that the SOC of graphene layers, spin pumping generated pure spin current, and spin transport efficiency at the interfaces play a pivotal role here. We estimate the spin-mixing conductance associated with the spin-pumping effect to be approximately 0.8×10^{15} cm^{-2}. This indicates that interfaces with monolayer graphene and graphite support better transport and absorption of angular momentum from the CoGd layer, which is hindered in the case of bilayer-, trilayer-, and FL-graphene. We also report the presence of other extrinsic factors that increase the effective damping in a nonlinear fashion for the low field regime and are eliminated at the high field regime. Atomically thin graphene with elevated extrinsic SOC supports efficient absorption and transportation of carriers across the interface within a spintronic device. Relatively thicker graphite with large intrinsic SOC and distinct thermal properties also incorporates various functionalities to the adjacent magnetic layers. Our study highlights the fact that these 2-D materials in different forms can be extremely beneficial for expediting the dynamics of magnetic layers in ultrafast time scales. Specifically, we foresee long-term benefits of this close association between graphene and ferrimagnetic systems for the future spintronic applications, such as, magnetic analogue for wearable electronics, sensors that harness renewable energy,[64] magnetic tunnel junctions,[5] THz emitters,[65] graphene interconnects in all-spin logic devices,[66] and "spinterfacing" with magnetic heterostructures important for "organic spintronics",[67] etc.

EXPERIMENTAL SECTION

Sample Fabrication. The exfoliation of graphene using a Scotch tape is a very easy, cost-effective, and popular method. It does not suffer from additional complexities, such as side reactions with oxygen or exposure to several impurities experienced during the chemical exfoliation method. At first, metallic markers are lithographically patterned on a 7 mm × 7 mm silicon substrate coated with 300 nm-thick SiO_2. This helps in identification of the graphene flakes on the substrate later. The sample is cleaned with a highly reactive reagent to remove organic residue and dirt. The surface is then converted into a hydrophilic one. Then, the graphene flakes of different layer numbers are mechanically exfoliated and transferred on to the substrate. It is again treated with a quick rinse of acetone and IPA followed by dry nitrogen purging to remove any impurity after exfoliation.

An amorphous film of CoGd (10 nm)/Ta (4 nm) is deposited by the DC magnetron sputtering technique on a Si/SiO_2/graphene substrate at ultrahigh vacuum (base pressure $\sim 5 \times 10^{-8}$ Torr). The thicknesses of the CoGd and Ta layers are calculated from the deposition rate and time. The CoGd alloy is deposited by cosputtering of Co and Gd targets. We use the following physical parameters for the calculation of elemental composition. The densities of Co (ρ_{Co}) and Gd (ρ_{Gd}) are 8.9 g/cm^3 and 7.8 g/cm^3 respectively. The atomic weights of Co (A_{Co}) and Gd (A_{Gd}) are 58.93 and 157.25 respectively. The atomic ratios of Co and Gd are calculated from the following formula:

$$\frac{r_{Co}\rho_{Co}A_{Gd}}{r_{Co}\rho_{Co}A_{Gd} + r_{Gd}\rho_{Gd}A_{Co}} : \frac{r_{Gd}\rho_{Gd}A_{Co}}{r_{Co}\rho_{Co}A_{Gd} + r_{Gd}\rho_{Gd}A_{Co}}$$

where r_{Co} and are r_{Gd} are the deposition rate of Co and Gd at the sputtered power of 35 and 15 W respectively for 3 min 54 s. The rates are calibrated to be 0.20 and 0.21 Å/s, respectively. Using the above-mentioned formula, we estimate the composition of the CoGd alloy to be $Co_{74}Gd_{26}$. This higher composition of Gd shifts the compensation point above room temperature. Ta is deposited at 30 W power for 2 min and 12 s. This capping layer prevents the magnetic surface from any environmental degradation. The thickness of the magnetic film is calibrated and optimized beforehand for the above-mentioned deposition condition.

Micro-Raman Spectroscopy Measurement. The micro-Raman scattering experiment[68] was carried out using a Renishaw InVis Raman microscope. An argon laser with wavelength at 514 nm was employed as the excitation source. A 100× objective with a numerical aperture of 0.85 was used to achieve the laser spot with a diameter of around 1 μm. The light spot is tightly focused on the middle of each flake to achieve the Raman intensity with a reasonably high signal-to-noise ratio. The grating specification is 1800 lines/mm. The detector is a Renishaw Centrus 07GM43. We performed spatial mapping of defect density with a resolution of about 1 μm, and an area of about 40 μm × 40 μm was scanned for each run.

Optical Pump−Probe Measurement. We used a single-color pump−probe technique in the TRMOKE experiment.[69] The laser beam was generated from a regeneratively amplified Ti-Sapphire laser source (Coherent model RegA: $\lambda \approx 800$ nm, pulse width ~90 fs, repetition rate ≈ 252 kHz) and was split into a pump (higher energy) and probe beam (lower energy) by a polarizing beam splitter. The intense beam hits the sample in a noncollinear fashion to excite the magnetization dynamics, and the probe beam is tightly focused within the pump spot to ensure the detection of uniformly excited magnetization dynamics. The pump and probe spot diameters are ~140 μm and ~3 μm, respectively. The time delay between the pump and probe pulses was modified by using a mechanical delay stage. After the linearly polarized probe beam gets reflected from the sample, it passes through an analyzer which is kept at near extinction before going into a photodetector (PD). The PD measures the intensity which is then fed into the lock-in amplifier. The pump beam is modulated with a mechanical chopper at 419 Hz frequency, which is then used as the reference frequency of the lock-in amplifier for the detection of the time-delayed signal in a phase-sensitive manner. To ensure the position of pump and probe spots on the region containing

https://doi.org/10.1021/acsnano.2c02899
ACS Nano 2022, 16, 9620−9630

graphene flakes, we mounted the sample to a X-Y-Z translational stage having considerably good precision. The probe fluence was kept fixed at 0.5 mJ/cm^2, and the pump fluence was fixed at 3.0 mJ/cm^2 throughout the experiment. In this moderate fluence regime, we did not observed any heating in the experimental data. A large static field was applied to saturate the samples along the direction of the field with almost 15° OOP tilt. Magnitude of the field was varied during the field-dependent measurements. The time delay in this experiment was limited to 1 ns due to the physical length of the delay stage. This time window was enough to record the time-resolved profile of the polar Kerr signal from femtosecond to nanosecond time scales accommodating multiple oscillations.

ASSOCIATED CONTENT

Supporting Information

The Supporting Information is available free of charge at https://pubs.acs.org/doi/10.1021/acsnano.2c02899.

Analysis of the results obtained from Raman spectroscopy measurements; surface properties investigated by the atomic force microscopy (AFM) technique; modeling of the ultrafast demagnetization phenomenon; modeling of precessional dynamics; thermal properties of the graphene layers; qualitative analysis of the heat transportation in the substrate/graphene/CoGd system correlating the slow remagnetization phenomenon; determination of the spin-chemical potential and spin-mixing conductance; bias magnetic field-dependent precessional dynamics (PDF)

AUTHOR INFORMATION

Corresponding Author

Jeffrey Bokor − *Department of Electrical Engineering and Computer Sciences, University of California, Berkeley, California 94720, United States; Materials Sciences Division, Lawrence Berkeley National Laboratory, Berkeley, California 94720, United States;* orcid.org/0000-0002-4541-0156; Email: jbokor@berkeley.edu

Authors

Sucheta Mondal − *Department of Electrical Engineering and Computer Sciences, University of California, Berkeley, California 94720, United States;* orcid.org/0000-0002-2355-2540

Yuxuan Lin − *Department of Electrical Engineering and Computer Sciences, University of California, Berkeley, California 94720, United States;* orcid.org/0000-0003-0638-2620

Debanjan Polley − *Department of Electrical Engineering and Computer Sciences, University of California, Berkeley, California 94720, United States; Materials Sciences Division, Lawrence Berkeley National Laboratory, Berkeley, California 94720, United States*

Cong Su − *Kavli Energy Nanoscience Institute and Department of Physics, University of California, Berkeley, California 94720, United States; Materials Sciences Division, Lawrence Berkeley National Laboratory, Berkeley, California 94720, United States;* orcid.org/0000-0002-7198-0259

Alex Zettl − *Kavli Energy Nanoscience Institute and Department of Physics, University of California, Berkeley, California 94720, United States; Materials Sciences Division, Lawrence Berkeley National Laboratory, Berkeley, California 94720, United States*

Sayeef Salahuddin − *Department of Electrical Engineering and Computer Sciences, University of California, Berkeley, California 94720, United States; Materials Sciences Division, Lawrence Berkeley National Laboratory, Berkeley, California 94720, United States*

Complete contact information is available at: https://pubs.acs.org/10.1021/acsnano.2c02899

Author Contributions

S.M. and J.B. proposed the project and designed the experiment, Y.L. performed the graphene exfoliation process, D.P. and S.S. deposited the CoGd film in sputtering. S.M. and S.S. performed the vibrating sample magnetometry measurements on the bare CoGd film. Y.L., C.S., and A.Z. performed the Raman scattering measurements on graphene layers before and after the deposition of magnetic film. S.M. performed the atomic force microscopy measurements. S.M. and J.B. performed the TRMOKE measurements. S.M. analyzed the data, prepared the figures, and wrote the draft of the manuscript after consultation with J.B. The manuscript was finalized through contributions of all authors. All authors have given approval to the final version of the manuscript.

Notes

The authors declare no competing financial interest.

ACKNOWLEDGMENTS

This work was primarily supported by the Director, Office of Science, Office of Basic Energy Sciences, Materials Sciences and Engineering Division, of the U.S. Department of Energy under Contract No. DE-AC02-05-CH11231 within the Nonequilibrium Magnetic Materials Program (MSMAG). This work was also supported by ASCENT (one of the SRC/DARPA supported centers within the JUMP initiative) (sample preparation), the National Science Foundation Center for Energy Efficient Electronics Science, and the Berkeley Emerging Technology Research (BETR) Center (data analysis). C.S. and A.Z. acknowledge support from the Director, Office of Science, Office of Basic Energy Sciences, Materials Sciences and Engineering Division, of the U.S. Department of Energy, under Contract No. DE-AC02-05-CH11231 within the van der Waals Heterostructures Program (KCWF16), which provided for the Raman characterization.

REFERENCES

(1) Tombros, N.; Jozsa, C.; Popinciuc, M.; Jonkman, H. T.; Van Wees, B. J. Electronic Spin Transport and Spin Precession in Single Graphene Layers at Room Temperature. *Nature* **2007**, *448*, 571−574.

(2) Han, W.; Pi, K.; McCreary, K. M.; Li, Y.; Wong, J. J. I.; Swartz, A. G.; Kawakami, R. K. Tunneling Spin Injection into Single Layer Graphene. *Phys. Rev. Lett.* **2010**, *105*, 167202.

(3) Yang, T. Y.; Balakrishnan, J.; Volmer, F.; Avsar, A.; Jaiswal, M.; Samm, J.; Ali, S. R.; Pachoud, A.; Zeng, M.; Popinciuc, M.; Güntherodt, G.; Beschoten, B.; Özyilmaz, B. Observation of Long Spin-Relaxation Times in Bilayer Graphene at Room Temperature. *Phys. Rev. Lett.* **2011**, *107*, 047206.

(4) Dery, H.; Wu, H.; Ciftcioglu, B.; Huang, M.; Song, Y.; Kawakami, R.; Shi, J.; Krivorotov, I.; Žutić, I.; Sham, L. J. Nanospintronics Based on Magnetologic Gates. *IEEE Trans. Electron Devices* **2012**, *59*, 259−262.

(5) Cobas, E.; Friedman, A. L.; Van'T Erve, O. M. J.; Robinson, J. T.; Jonker, B. T. Graphene As a Tunnel Barrier: Graphene-Based Magnetic Tunnel Junctions. *Nano Lett.* **2012**, *12*, 3000−3004.

(6) Han, W.; Kawakami, R. K.; Gmitra, M.; Fabian, J. Graphene Spintronics. *Nat. Nanotechnol.* **2014**, *9*, 794−807.

(7) Novoselov, K. S.; Geim, A. K.; Morozov, S. V.; Jiang, D.; Zhang, Y.; Dubonos, S. V.; Grigorieva, I. V.; Firsov, A. A. Electric Field Effect in Atomically Thin Carbon Films. *Science* **2004**, *306*, 666−669.
(8) Geim, A. K.; Novoselov, K. S. The Rise of Graphene. *Nat. Mater.* **2007**, *6*, 183−191.
(9) Castro Neto, A. H.; Guinea, F.; Peres, N. M. R.; Novoselov, K. S.; Geim, A. K. The Electronic Properties of Graphene. *Rev. Mod. Phys.* **2009**, *81*, 109−162.
(10) Das Sarma, S.; Adam, S.; Hwang, E. H.; Rossi, E. Electronic Transport in Two-Dimensional Graphene. *Rev. Mod. Phys.* **2011**, *83*, 407−470.
(11) Sang, M.; Shin, J.; Kim, K.; Yu, K. J. Electronic and Thermal Properties of Graphene and Recent Advances in Graphene Based Electronics Applications. *Nanomaterials* **2019**, *9*, 374.
(12) Mak, K. F.; Sfeir, M. Y.; Misewich, J. A.; Heinz, T. F. The Evolution of Electronic Structure in Few-Layer Graphene Revealed by Optical Spectroscopy. *Proc. Natl. Acad. Sci. U. S. A.* **2010**, *107*, 14999−15004.
(13) Guinea, F. Spin-Orbit Coupling in a Graphene Bilayer and in Graphite. *New J. Phys.* **2010**, *12*, 083063.
(14) Weeks, C.; Hu, J.; Alicea, J.; Franz, M.; Wu, R. Engineering a Robust Quantum Spin Hall State in Graphene *via* Adatom Deposition. *Phys. Rev. X* **2011**, *1*, 021001.
(15) Castro Neto, A. H.; Guinea, F. Impurity-Induced Spin-Orbit Coupling in Graphene. *Phys. Rev. Lett.* **2009**, *103*, 026804.
(16) Avsar, A.; Tan, J. Y.; Taychatanapat, T.; Balakrishnan, J.; Koon, G. K. W.; Yeo, Y.; Lahiri, J.; Carvalho, A.; Rodin, A. S.; O'Farrell, E. C. T.; Eda, G.; Castro Neto, A. H.; Özyilmaz, B. Spin-Orbit Proximity Effect in Graphene. *Nat. Commun.* **2014**, *5*, 1−6.
(17) Bertoni, G.; Calmels, L.; Altibelli, A.; Serin, V. First-Principles Calculation of the Electronic Structure and EELS Spectra at the Graphene/Ni(111) Interface. *Phys. Rev. B* **2005**, *71*, 075402.
(18) Matsumoto, Y.; Entani, S.; Koide, A.; Ohtomo, M.; Avramov, P. V.; Naramoto, H.; Amemiya, K.; Fujikawa, T.; Sakai, S. Spin Orientation Transition across the Single-Layer Graphene/Nickel Thin Film Interface. *J. Mater. Chem. C* **2013**, *1*, 5533−5537.
(19) Mondal, A. K.; Majumder, S.; Sahoo, S.; Panda, S. N.; Sinha, S.; Barman, A. Defect-Density- and Rashba-Shift-Induced Interfacial Dzyaloshinskii-Moriya Interaction and Spin Pumping in Single-Layer Graphene/$Co_{20}Fe_{60}B_{20}$ Heterostructures: Implications for New-Generation Spintronics. *ACS Appl. Nano Mater.* **2022**, *5*, 5056−5063.
(20) Abtew, T.; Shih, B. C.; Banerjee, S.; Zhang, P. Graphene-Ferromagnet Interfaces: Hybridization, Magnetization and Charge Transfer. *Nanoscale* **2013**, *5*, 1902−1909.
(21) Kane, C. L.; Mele, E. J. Quantum Spin Hall Effect in Graphene. *Phys. Rev. Lett.* **2005**, *95*, 226801.
(22) Anadón, A.; Gudín, A.; Guerrero, R.; Arnay, I.; Guedeja-Marron, A.; Jiménez-Cavero, P.; Díez Toledano, J. M.; Ajejas, F.; Varela, M.; Petit-Watelot, S.; Lucas, I.; Morellón, L.; Algarabel, P. A.; Ibarra, M. R.; Miranda, R.; Camarero, J.; Rojas-Sánchez, J. C.; Perna, P. Engineering the Spin Conversion in Graphene Monolayer Epitaxial Structures. *APL Mater.* **2021**, *9*, 061113.
(23) Idzuchi, H.; Iihama, S.; Shimura, M.; Kumatani, A.; Mizukami, S.; Chen, Y. P. Spin Injection Characteristics of Py/Graphene/Pt by Gigahertz and Terahertz Magnetization Dynamics Driven by Femtosecond Laser Pulse. *AIP Adv.* **2021**, *11*, 015321.
(24) Sinha, S.; Pan, S.; Choudhury, S.; Sinha, J.; Barman, A. Extrinsic Spin-Orbit Coupling-Induced Large Modulation of Gilbert Damping Coefficient in CoFeB Thin Film on the Graphene Stack with Different Defect Density. *J. Phys. Chem. C* **2017**, *121*, 17442−17449.
(25) Panda, S. N.; Majumder, S.; Choudhury, S.; Bhattacharya, A.; Sinha, S.; Barman, A. Femtosecond Laser-Induced Spin Dynamics in Single-Layer Graphene/CoFeB Thin Films. *Nanoscale* **2021**, *13*, 13709−13718.
(26) Panda, S. N.; Mondal, S.; Sinha, J.; Choudhury, S.; Barman, A. All-Optical Detection of Interfacial Spin Transparency from Spin Pumping in b-Ta/CoFeB Thin Films. *Sci. Adv.* **2019**, *5*, No. eaav7200.
(27) Patra, A. K.; Singh, S.; Barin, B.; Lee, Y.; Ahn, J. H.; Del Barco, E.; Mucciolo, E. R.; Özyilmaz, B. Dynamic Spin Injection into Chemical Vapor Deposited Graphene. *Appl. Phys. Lett.* **2012**, *101*, 162407.
(28) Bigot, J. Y.; Beaurepaire, E.; Daunois, A.; Merle, J. C. Spin Dynamics in Ferromagnetic Nickel Films. *Springer Ser. Chem. Phys.* **1996**, *62*, 414−415.
(29) van Kampen, M.; Jozsa, C.; Kohlhepp, J. T.; LeClair, P.; Lagae, L.; de Jonge, W. J. M.; Koopmans, B. All-Optical Probe of Coherent Spin Waves. *Phys. Rev. Lett.* **2002**, *88*, 227201.
(30) Koopmans, B.; Malinowski, G.; Dalla Longa, F.; Steiauf, D.; Fähnle, M.; Roth, T.; Cinchetti, M.; Aeschlimann, M. Explaining the Paradoxical Diversity of Ultrafast Laser-Induced Demagnetization. *Nat. Mater.* **2010**, *9*, 259−265.
(31) Stanciu, C. D.; Kimel, A. V.; Hansteen, F.; Tsukamoto, A.; Itoh, A.; Kirilyuk, A.; Rasing, T. Ultrafast Spin Dynamics across Compensation Points in Ferrimagnetic GdFeCo: The Role of Angular Momentum Compensation. *Phys. Rev. B* **2006**, *73*, No. 220402(R).
(32) Mondal, S.; Talapatra, A.; Arout Chelvane, J.; Mohanty, J. R.; Barman, A. Role of Magnetic Anisotropy in the Ultrafast Magnetization Dynamics of Gd-Fe Thin Films of Different Thicknesses. *Phys. Rev. B* **2019**, *100*, 054436.
(33) Stanciu, C. D.; Hansteen, F.; Kimel, A. V.; Kirilyuk, A.; Tsukamoto, A.; Itoh, A.; Rasing, T. All-Optical Magnetic Recording with Circularly Polarized Light. *Phys. Rev. Lett.* **2007**, *99*, 047601.
(34) Radu, I.; Vahaplar, K.; Stamm, C.; Kachel, T.; Pontius, N.; Dürr, H. A.; Ostler, T. A.; Barker, J.; Evans, R. F. L.; Chantrell, R. W.; Tsukamoto, A.; Itoh, A.; Kirilyuk, A.; Rasing, T.; Kimel, A. V. Transient Ferromagnetic-like State Mediating Ultrafast Reversal of Antiferromagnetically Coupled Spins. *Nature* **2011**, *472*, 205−209.
(35) Yang, Y.; Wilson, R. B.; Gorchon, J.; Lambert, C. H.; Salahuddin, S.; Bokor, J. Ultrafast Magnetization Reversal by Picosecond Electrical Pulses. *Sci. Adv.* **2017**, *3*, No. e1603117.
(36) Wang, L.; Cheng, H.; Li, P.; Liu, Y.; van Hees, Y. L. W.; Lavrijsen, R.; Lin, X.; Cao, K.; Koopmans, B.; Zhao, W. Picosecond Switching of Optomagnetic Tunnel Junctions. *arXiv* 2020, *03621*, https://arxiv.org/abs/2011.03612 (accessed March 23, 2022).
(37) Chen, J. Y.; He, L.; Wang, J. P.; Li, M. All-Optical Switching of Magnetic Tunnel Junctions with Single Subpicosecond Laser Pulses. *Phys. Rev. Appl.* **2017**, *7*, 021001.
(38) Yang, H.; Vu, A. D.; Hallal, A.; Rougemaille, N.; Coraux, J.; Chen, G.; Schmid, A. K.; Chshiev, M. Anatomy and Giant Enhancement of the Perpendicular Magnetic Anisotropy of Cobalt-Graphene Heterostructures. *Nano Lett.* **2016**, *16*, 145−151.
(39) Malard, L. M.; Pimenta, M. A.; Dresselhaus, G.; Dresselhaus, M. S. Raman Spectroscopy in Graphene. *Phys. Rep.* **2009**, *473*, 51−87.
(40) Gupta, A.; Chen, G.; Joshi, P.; Tadigadapa, S.; Eklund, P. C. Raman Scattering from High-Frequency Phonons in Supported n-Graphene Layer Films. *Nano Lett.* **2006**, *6*, 2667−2673.
(41) Dalla Longa, F.; Kohlhepp, J. T.; De Jonge, W. J. M.; Koopmans, B. Influence of Photon Angular Momentum on Ultrafast Demagnetization in Nickel. *Phys. Rev. B* **2007**, *75*, 224431.
(42) Malinowski, G.; Dalla Longa, F.; Rietjens, J. H. H.; Paluskar, P. V.; Huijink, R.; Swagten, H. J. M.; Koopmans, B. Control of Speed and Efficiency of Ultrafast Demagnetization by Direct Transfer of Spin Angular Momentum. *Nat. Phys.* **2008**, *4*, 855−858.
(43) Landau, L.; Lifshitz, E. On the Theory of the Dispersion of Magnetic Permeability in Ferromagnetic Bodies. *Perspect. Theor. Phys.* **1992**, *169*, 51−65.
(44) Gilbert, T. L. A Phenomenological Theory of Damping in Ferromagnetic Materials. *IEEE Trans. Magn.* **2004**, *40*, 3443−3449.
(45) Mondal, S.; Barman, A. Laser Controlled Spin Dynamics of Ferromagnetic Thin Film from Femtosecond to Nanosecond Timescale. *Phys. Rev. Appl.* **2018**, *10*, 054037.
(46) Binder, M.; Weber, A.; Mosendz, O.; Woltersdorf, G.; Izquierdo, M.; Neudecker, I.; Dahn, J. R.; Hatchard, T. D.; Thiele, J. U.; Back, C. H.; Scheinfein, M. R. Magnetization Dynamics of the Ferrimagnet CoGd near the Compensation of Magnetization and Angular Momentum. *Phys. Rev. B* **2006**, *74*, 134404.
(47) Dedkov, Y. S.; Fonin, M. Electronic and Magnetic Properties of the Graphene-Ferromagnet Interface. *New J. Phys.* **2010**, *12*, 125004.

https://doi.org/10.1021/acsnano.2c02899
ACS Nano 2022, 16, 9620−9630

(48) Huertas-Hernando, D.; Guinea, F.; Brataas, A. Spin-Orbit Coupling in Curved Graphene, Fullerenes, Nanotubes, and Nanotube Caps. *Phys. Rev. B* **2006**, *74*, 155426.
(49) Massicotte, M.; Soavi, G.; Principi, A.; Tielrooij, K. J. Hot Carriers in Graphene-Fundamentals and Applications. *Nanoscale* **2021**, *13*, 8376−8411.
(50) Pop, E.; Varshney, V.; Roy, A. K. Thermal Properties of Graphene: Fundamentals and Applications. *MRS Bull.* **2012**, *37*, 1273−1281.
(51) Jang, W.; Chen, Z.; Bao, W.; Lau, C. N.; Dames, C. Thickness-Dependent Thermal Conductivity of Encased Graphene and Ultrathin Graphite. *Nano Lett.* **2010**, *10*, 3909−3913.
(52) Koh, Y. K.; Bae, M. H.; Cahill, D. G.; Pop, E. Heat Conduction across Monolayer and Few-Layer Graphenes. *Nano Lett.* **2010**, *10*, 4363−4368.
(53) Harb, M.; Von Korff Schmising, C.; Enquist, H.; Jurgilaitis, A.; Maximov, I.; Shvets, P. V.; Obraztsov, A. N.; Khakhulin, D.; Wulff, M.; Larsson, J. The C-Axis Thermal Conductivity of Graphite Film of Nanometer Thickness Measured by Time Resolved X-Ray Diffraction. *Appl. Phys. Lett.* **2012**, *101*, 233108.
(54) Swartz, E. T.; Pohl, R. O. Thermal Boundary Resistance. *Rev. Mod. Phys.* **1989**, *61*, 605−668.
(55) Braun, J. L.; Szwejkowski, C. J.; Giri, A.; Hopkins, P. E. On the Steady-State Temperature Rise during Laser Heating of Multilayer Thin Films in Optical Pump-probe Techniques. *J. Heat Transfer* **2018**, *140*, 052801.
(56) Liu, W. Q.; Wang, W. Y.; Wang, J. J.; Wang, F. Q.; Lu, C.; Jin, F.; Zhang, A.; Zhang, Q. M.; Laan, G. Van Der; Xu, Y. B.; Li, Q. X.; Zhang, R. Atomic-Scale Interfacial Magnetism in Fe/Graphene Heterojunction. *Sci. Rep.* **2015**, *5*, 11911.
(57) Gannett, W.; Keller, M. W.; Nembach, H. T.; Silva, T. J.; Chiaramonti, A. N. Suppression of Spin Pumping between $Ni_{80}Fe_{20}$ and Cu by a Graphene Interlayer. *J. Appl. Phys.* **2015**, *117*, 213907.
(58) Zhang, W.; Liu, Q.; Yuan, Z.; Xia, K.; He, W.; Zhan, Q. F.; Zhang, X. Q.; Cheng, Z. H. Enhancement of Ultrafast Demagnetization Rate and Gilbert Damping Driven by Femtosecond Laser-Induced Spin Currents in $Fe_{81}Ga_{19}/Ir_{20}Mn_{80}$ Bilayers. *Phys. Rev. B* **2019**, *100*, 104412.
(59) Song, J. C. W.; Rudner, M. S.; Marcus, C. M.; Levitov, L. S. Hot Carrier Transport and Photocurrent Response in Graphene. *Nano Lett.* **2011**, *11*, 4688−4692.
(60) Zhang, W.; He, W.; Zhang, X. Q.; Cheng, Z. H.; Teng, J.; Fähnle, M. Unifying Ultrafast Demagnetization and Intrinsic Gilbert Damping in Co/Ni Bilayers with Electronic Relaxation near the Fermi Surface. *Phys. Rev. B* **2017**, *96*, 220415.
(61) Konschuh, S.; Gmitra, M.; Kochan, D.; Fabian, J. Theory of Spin-Orbit Coupling in Bilayer Graphene. *Phys. Rev. B* **2012**, *85*, 115423.
(62) Park, J. H.; Lee, H. J. Out-of-Plane Magnetoresistance in Ferromagnet/Graphene/Ferromagnet Spin-Valve Junctions. *Phys. Rev. B* **2014**, *89*, 165417.
(63) Hurben, M. J.; Patton, C. E. Theory of Two Magnon Scattering Microwave Relaxation and Ferromagnetic Resonance Linewidth in Magnetic Thin Films. *J. Appl. Phys.* **1998**, *83*, 4344−4365.
(64) Lin, Y.; Li, X.; Xie, D.; Feng, T.; Chen, Y.; Song, R.; Tian, H.; Ren, T.; Zhong, M.; Wang, K.; Zhu, H. Graphene/Semiconductor Heterojunction Solar Cells with Modulated Antireflection and Graphene Work Function. *Energy Environ. Sci.* **2013**, *6*, 108−115.
(65) Hunter, N.; Mayorov, A. S.; Wood, C. D.; Russell, C.; Li, L.; Linfield, E. H.; Davies, A. G.; Cunningham, J. E. On-Chip Picosecond Pulse Detection and Generation Using Graphene Photoconductive Switches. *Nano Lett.* **2015**, *15*, 1591−1596.
(66) Behin-Aein, B.; Datta, D.; Salahuddin, S.; Datta, S. Proposal for an All-Spin Logic Device with Built-in Memory. *Nat. Nanotechnol.* **2010**, *5*, 266−270.
(67) Mallik, S.; Mattauch, S.; Dalai, M. K.; Brückel, T.; Bedanta, S. Effect of Magnetic Fullerene on Magnetization Reversal Created at the Fe/C_{60} Interface. *Sci. Rep.* **2018**, *8*, 5515.
(68) Shen, P. C.; Su, C.; Lin, Y.; Chou, A. S.; Cheng, C. C.; Park, J. H.; Chiu, M. H.; Lu, A. Y.; Tang, H. L.; Tavakoli, M. M.; Pitner, G.; Ji, X.; Cai, Z.; Mao, N.; Wang, J.; Tung, V.; Li, J.; Bokor, J.; Zettl, A.; Wu, C. I.; Palacios, T.; Li, L. J.; Kong, J. Ultralow Contact Resistance between Semimetal and Monolayer Semiconductors. *Nature* **2021**, *593*, 211−217.
(69) El-Ghazaly, A.; Tran, B.; Ceballos, A.; Lambert, C. H.; Pattabi, A.; Salahuddin, S.; Hellman, F.; Bokor, J. Ultrafast Magnetization Switching in Nanoscale Magnetic Dots. *Appl. Phys. Lett.* **2019**, *114*, 232407.

https://doi.org/10.1021/acsnano.2c02899
ACS Nano 2022, 16, 9620−9630